J Nanopart Res (2017) 19:104
DOI 10.1007/s11051-017-3755-4

RESEARCH PAPER

Nanoparticle transport in water-unsaturated porous media: effects of solution ionic strength and flow rate

Dieuseul Prédélus · Laurent Lassabatere · Cédric Louis · Hélène Gehan · Thomas Brichart · Thierry Winiarski · Rafael Angulo-Jaramillo

Received: 14 November 2016 / Accepted: 23 January 2017

Abstract This paper presents the influence of ionic strength and flow on nanoparticle (NP) retention rate in an unsaturated calcareous medium, originating from a heterogeneous glaciofluvial deposit of the region of Lyon (France). Laboratory columns 10 cm in diameter and 30 cm in length were used. Silica nanoparticles (Au-SiO_2-FluoNPs), with hydrodynamic diameter ranging from 50 to 60 nm and labeled with fluorescein derivatives, were used to simulate particle transport, and bromide was used to characterize flow. Three flow rates and five different ionic strengths were tested. The transfer model based on fractionation of water into mobile and immobile fractions was coupled with the attachment/detachment model to fit NPs breakthrough curves. The results show that increasing flow velocity induces a decrease in nanoparticle retention, probably as the result of several physical but also geochemical factors. The results show that NPs retention increases with ionic strength. However, an inversion of retention occurs for ionic strength >5.10^{-2} M, which has been scarcely observed in previous studies. The measure of zeta potential and DLVO calculations show that NPs may sorb on both solid-water and air-water interfaces. NPs size distribution shows the potential for nanoparticle agglomeration mostly at low pH, leading to entrapment in the soil pores. These mechanisms are highly sensitive to both hydrodynamic and geochemical conditions, which explains their high sensitivity to flow rates and ionic strength.

Keywords Flow rate · Ionic strength · Modeling · Nanoparticles · Unsaturated soil · Environmental pollutants · Colloids

D. Prédélus · L. Lassabatere (✉) · T. Winiarski · R. Angulo-Jaramillo
Université de Lyon, Laboratoire d'Ecologie des Hydrosystèmes Naturels et Anthropisés, LEHNA, UMR 5023 CNRS, ENTPE, UCB-Lyon-1, Rue Maurice Audin, 69518 Vaulx-en-Velin, France
e-mail: laurent.lassabatere@entpe.fr

C. Louis · H. Gehan
Nano-H S.A.S., 2 place de l'Europe, Bâtiment A, Parc d'activité VALAD, 38070 Saint Quentin Fallavier 3- UFPE, France

T. Brichart
Institut Lumière Matière, UMR 5306 CNRS, Université Lyon 1-CNRS, Villeurbanne Cedex, France

Introduction

In recent years, the transport of nanoparticles (NPs) in porous media and soils has become a subject of great concern since they can sorb contaminants, due to their high specific surface, and then carry these contaminants along large distances (Ryan et al. 1998; McGechan and Lewis 2002). NPs are characterized by a mobility often superior or equal to that of solutes (Wan and Wilson 1994; Lamy et al. 2013). Three hypotheses can explain this phenomenon. Firstly, NPs have a low molecular diffusion coefficient, which excludes them from areas with low flow rate. Secondly, NPs can be excluded from some of the micro-porosity where the pore size is smaller than their own size (Grolimund et al. 1998; Kretzschmar et al. 1999; Sirivithayapakorn and Keller

Published online: 10 March 2017

2003). Thirdly, in pores of a sufficient radius, NPs are more likely transported to the pore center where the flow velocity is higher in contrast to solutes, which are drawn towards the pore walls (Powelson et al. 1993). This phenomenon known as steric exclusion is due to NPs size, which prevents them from getting closer to the soil particle walls where fluid velocity is lower. This hydrodynamic effect results in a higher average flow rate of NPs than that of the carrier fluid (Keller and Auset 2007). Larger NPs are carried at higher rates and cannot approach the pore walls due to their dimension (Lamy et al. 2013). These factors explain why NPs constitute a great risk for soil quality in the vadose zone as well as groundwater quality. Consequently, it is important to identify the mechanisms of transfer and retention of NPs as well as environmental factors that influence their fate in the unsaturated zone.

In addition to the conventional NPs transportation processes (convection, diffusion, and dispersion), several retention mechanisms may occur: adsorption, attachment to the air-water (AWI) or solid-water (SWI) interfaces and straining, referring to entrapment of NPs, or NPs agglomerates in soil pores (Tian et al. 2012). The attachment of NPs on air-water or solid-water interfaces is caused by electrostatic forces or surface tension. It depends on the pH and the ionic strength of solution and also the surface properties of NPs (DeNovio et al. 2004; Torkzaban et al. 2006b). However, the NPs are not strongly attached and can be remobilized easily or can be conveyed to immobile zones by hydrodynamic forces (Johnson et al. 2007; Torkzaban et al. 2008). Straining is the mechanical blocking of NPs in pores of smaller size than NPs sizes including areas where local fluid velocity is non-zero (Bradford and Bettahar 2006). Straining is water saturation dependent with more straining under unsaturated conditions as capillary forces drive water and NPs in regions of smaller pore size (Chen et al. 2008a, b; Zang et al. 2012). As an additional mechanism, triple points of the interface water-air-solid form areas where low flow rate creates additional causes for trapping NPs. Torkzaban et al. (2008) considered triple point retention as an additional form of straining. In concomitance with the mechanisms described above, the agglomeration of NPs can play a significant role. Agglomeration of NPs results from interactions between the NPs themselves (Solovitch et al. 2010) and is strongly dependent on the chemical properties of the fluid carrying NPs, and, in particular, ionic strength and pH. NPs agglomeration forms larger objects that can be trapped more easily by straining, given their larger sizes in comparison to isolated NPs.

Chemical characteristics of interstitial water may play a significant role on the fate of NPs. Indeed, most of the mechanisms described above are ionic strength and pH dependent. pH rules NPs and solid surface charges, thus impacting electrostatic attraction between NPs and soil particles and between NPs themselves. This effect may result in a significant impact on NPs attachment to air-water and solid-water interfaces as well as NPs agglomeration. Ionic strength also affects the electrostatic attraction by reducing the electrostatic double layer, thus favoring NPs agglomeration and NPs attraction to solid-water interface. It has been reported many times that ionic strength favors NPs retention (e.g., Jacobs et al. 2007; Fang et al. 2013).

Hydrodynamics must play a significant role as well. Bulk convection and dispersion of NPs in soils may depend on flow rates and flow patterns. Flow rate impacts pore water velocity and increases hydrodynamic forces at the local scale. In addition to this direct effect, flow rate may also impact water saturation under unsaturated conditions, which may in turn impact attachment to air-water interfaces (Torkzaban et al. 2006a, b). Flow pattern and in particular flow homogeneity is known to rule the access of solutes to adsorption sites (Lassabatere et al. 2004; Lassabatere et al. 2007; Hanna et al. 2010) as well as the access of particles and colloids to trapping sites (Lamy et al. 2010; Lamy et al. 2013). In particular, heterogeneous flow reduces the access to sorption sites, thus decreasing retention. Clearly, modifications in hydrodynamic conditions, including flow rate, water content, and flow homogeneity, and their influences on NPs retention in soils must be considered and need to be investigated.

The objective of this work is to study the effect of ionic strength and flow rate on NPs retention in an unsaturated calcareous soil. The soil originates from a calcareous deposit that covers significant parts of the Rhône-Alpes region. This soil is known for its high buffer capacity and high pH (Lassabatere et al. 2007). It has already been the subject of several investigations for the fate of several pollutants (Lassabatere et al. 2007; Winiarski et al. 2013) including nanoparticles (Prédélus et al. 2014). The study of Prédélus et al. (2014) focused on the effect of soil particle size distribution on NPs retention and proposed several mechanisms for NPs retention in the studied soil. However, the identification of the mechanisms

responsible for NPs retention was not complete and leaching experiments were performed at one ionic strength and one injection flow rate only. The proposed study investigates the cases of several injection flow rates and solution ionic strengths. The experiments were conducted using laboratory columns, initially unsaturated and submitted to gravity-driven flow at several injection flow rates. Breakthrough curves (BTCs) and retention profiles were monitored and modeled using a transfer model including fractionation of water into two phases, mobile and immobile (MIM), and an attachment/detachment model for NPs retention. Fluorescent NPs, with a diameter ranging from 50 to 60 nm and labeled by a fluorescein derivative to ease their detection at column outlets and in columns, were those developed by Prédélus et al. (2014). These particles were characterized concerning their size distribution and Zeta potential to assess the potential for NPs agglomeration and for NPs adsorption onto soil-water or air-water interfaces (DLVO calculations).

Materials and methods

Studied material

The studied soil originates from the calcareous glaciofluvial deposit that covers most of the plains in the region of Lyon (France) and that is made mainly of the lithofacies referred to as Gcm,b (Goutaland et al. 2008). This lithofacies is composed of a mixture of sand and gravel. To ease replicability, the lithofacies was extracted and then sieved at two separate particle size fraction: sand (≤0.2 cm) and gravel (0.4–1.1 cm). Before construction of the columns, the material was reconstituted from separate particle size fractions in mass fraction 50%-50%. The particle size distribution of the material is typically bimodal with a mode corresponding to the gravel fraction and a second mode corresponding to the sandy matrix (Fig. 1a). On the basis of the model of Arya and Paris (1981), the corresponding pore size distribution was determined and the potential for NPs entrapment in soil pores was assessed considering the approach of Herzig et al. (1970). As the glaciofluvial deposit it originates from, the studied material has a high carbonate content (around 25%), a high pH (~8.65), and a strong buffer capacity (Lassabatere et al. 2007).

Bromide and nanoparticles

Neutral solution (S_0), made of sodium nitrate ($NaNO_3$) at 10^{-2} M, was used to moisturize the soil, saturate the columns, activate flow before the tracer, NPs injection experiments, and to wash the systems between successive injection experiments. Bromide was used to trace water flow and identify hydrodispersive parameters (see Lassabatere et al. 2004, 2007 for more details). Bromide concentration was fixed at 10^{-2} M and bromide was introduced as potassium bromide (KBr). The concentration of bromide was measured by ion chromatography (ICS 1100, Dionex ThermoScientific, Bannockburn, USA).

Studied NPs are composed of silica (Au-SiO_2-FluoNPs) labeled by fluorescein isothiocyanate (Fig. 1b). Each nanoparticle is made of a heart of gold of about 5 nm in diameter coated with a layer of polysiloxane (modified silica matrix) containing organic dyes. NPs' surface was grafted with specific functional hydroxyl groups (−OH) as well as gluconamide groups to keep them mono-dispersed in solutions. The hydrodynamic diameters of NPs are between 50 and 60 nm. The concentration of NPs was set at 0.2 g L^{-1} in $NaNO_3$ solution, which corresponds to approximately 1.08 10^{14} NPs L^{-1}. This concentration proved sufficient to get detectable and quantifiable concentrations in the columns and at the column outlets. Concentrations in liquids were determined by the measure of fluorescence intensity, using UV-visible fluorometer (Cary Eclipse BIO, Varian, Santa Clara, USA) with an excitation light set at 495 nm and detection centered around 515 nm. The ionic strengths of NPs solutions were fixed at five contrasted values (1, 10, 50, 100, and 200 mM) by adding sodium nitrate.

The agglomeration of nanoparticles was studied as a function of pH and ionic strength for the five solutions presented above. pH was modified by the addition of 0.12 M of pure HCl solution or 0.10 M of pure NaOH solution by a step increment of 0.6 for most solutions between 4 and 10. For the solution with ionic strength set at 10 mM, pH increments were reduced to 0.3. For each pH increment, the zeta potential of NPs and size distribution of NPs agglomerates were measured using a ZetaSizer Nano Z apparatus (Malvern, Westborough MA, USA). Zeta potential was used for DLVO calculations, to assess the potential for NPs attachment to the soil-water interface (SWI) and air-water interface (AWI) (Bradford and Torkzaban 2008; Chowdhury et al. 2011;

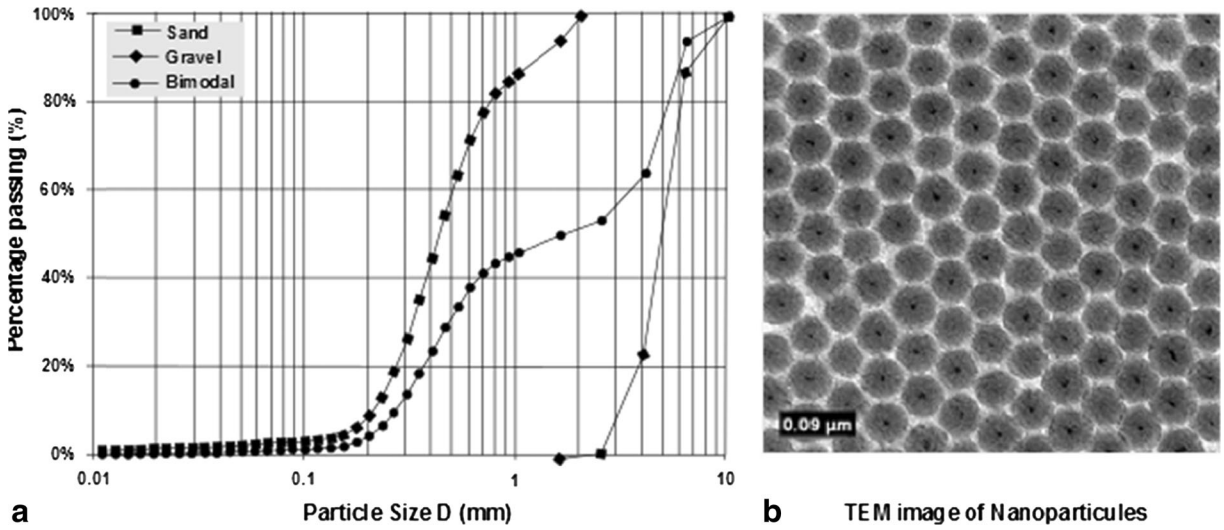

Fig. 1 Particle size distribution of the studied bimodal material obtained by mixing 50% by mass of sand and gravel (**a**); image of nanoparticles obtained by transmission electronic microscopy (TEM), each particle (*gray*) with a heart of gold that appears *black* (**b**)

Derjaguin and Landau 1941; Verwey and Overbeek 1955). Interaction profiles for the NPs attachment to SWI or AWI were developed assuming sphere-plate geometry and using the following equations (Chowdhury et al. 2011):

$$\varnothing_{tot}(h) = \varnothing_{vdw}(h) + \varnothing_{el}(h) \tag{1}$$

$$\varnothing_{vdw}(h) = -\frac{A\, r_p}{6\, h}\left[1 + \frac{14h}{\lambda}\right]^{-1} \tag{2}$$

$$\varnothing_{el}(h) = \pi\varepsilon_r\varepsilon_0 r_p\left(2\psi_p\psi_c ln\left[\frac{1+\exp(-\kappa h)}{1-\exp(-\kappa h)}\right]\right) + \left(\psi_p^2 + \psi_c^2\right) ln(1-\exp(-2\kappa h)) \tag{3}$$

where ϕ_{vdw} and ϕ_{el} are potentials related to Van der Waals and electrostatic forces, ϕ_{tot} stands for total potential, h is the distance between the sphere and the plane of the AWI or SWI interfaces, r_p is the radius of the particle, and λ is the characteristic wavelength (λ = 100 nm). A is the Hamaker constant, equal to 10^{-20} and -10^{-20} J for the SWI and AWI, respectively (Fang et al. 2013). ε_r is the dimensionless relative dielectric constant of the suspending liquid, ε_0 ($C^2\ J^{-1}\ m^{-1}$) is the permittivity of free space, ψ_p (V) is the surface potential of the nanoparticle, ψ_c (V) is the surface potential of the collector surface SWI or AWI (plane). For this study, the surface potential for the particles, ψ_p, was equaled to the measure of the zeta potential. The surface potential for the soil as collector surface, ψ_s, was equaled to the measure of the zeta potential of a soil suspension. For air, an average of surface potential of −25 mV was used, based on the study of Yang et al. (2001). Finally, κ (m^{-1}) is the inverse of the diffuse layer thickness, known as the Debye–Huckel parameter (Ruckenstein and Prieve 1976):

$$\kappa = \left[\frac{2I_s N_A\ 1000\ e^2}{\varepsilon_r\varepsilon_0 k_B T}\right]^{1/2} \tag{4}$$

I_S stands for ionic strength (mol L^{-1}), $N_A = 6.02\ 10^{23}$ (mol^{-1}) stands for Avogadro's number, $e = 1.602\ 10^{-19}$ (C) is the elementary charge, $k_B = 1.38\ 10^{-23}$ ($J\ K^{-1}$) is the Boltzmann constant, and T the fluid absolute temperature (K). Born repulsion, a short-range mechanism, was not considered in this study as discussed by several authors (e.g., Mitropoulou et al. 2013).

Column experiments

Polyvinyl chloride (PVC) laboratory columns, 10 cm in diameter and 30 cm in length, were used (Fig. 2). The material was moisturized at a water content of 7% (*w*/*w*) before embedment into columns by adding 3-cm-thick layers. Such procedure leads to a dry bulk density around 1.78 ± 0.04 g cm^{-3}. Glass beads of 0.5 cm in diameter were placed at the bottom and top of the

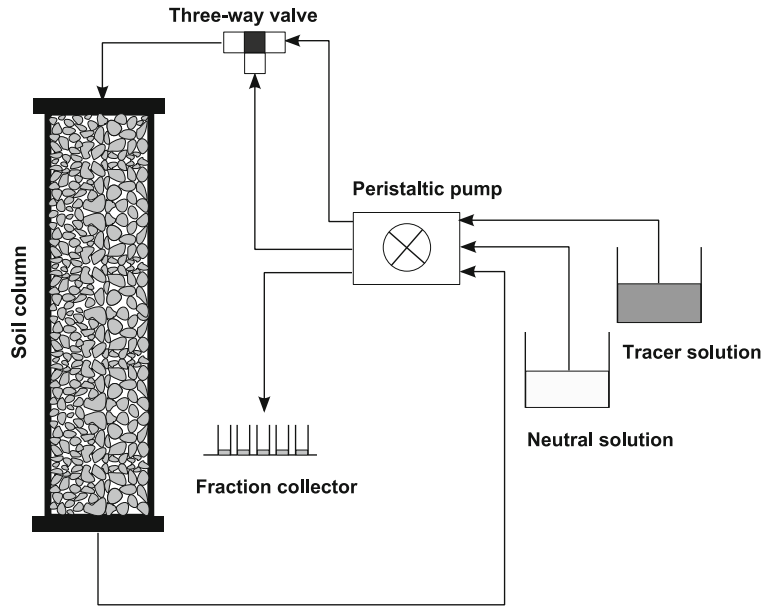

Fig. 2 Schematic diagram of leaching experimental set-up

column over a thickness of around 1.5 cm to ensure homogenization of fluxes at column outlets and inlets. PVC grids and 0.45-μm filters were added to reduce the leaching of fine particles. Before embedment, the column walls were coated with silicone grease to limit parasitic flow along the column walls.

To investigate successively the effect of both flow rate and ionic strength, column experiments were performed at three flow rates (0.025, 0.065, and 0.127 cm min^{-1}) for the injection of the solution with an ionic strength of 10 mM and at q = 0.127 cm min^{-1} for the injection of the five solutions (I_S = 1, 10, 50, 100, and 200 mM). The solutions were injected under unsaturated conditions, using gravity-driven flow. At the beginning of experiments, a neutral solution was injected at the top of the columns using peristaltic pumps to initiate flow. Water infiltrated into the systems, moisturized the soil, and after a given time, reached the bottom of columns. At that time, outlets were linked to peristaltic pumps to favor the extraction of water by suction. The peristaltic pumps upstream and downstream were set at the same flow rate to maintain steady state flow. Three-way valves were used to allow the change of solution without any flow disturbance. At the outlets, the pumps were linked to an automatic fraction collector (Gilson FC204, Middleton, USA) to collect samples every 30, 12, or 6 min depending on flowrates. Solutes were applied as a pulse mode with the injection of two thirds of the volume of water in columns (V_0) for both NPs and tracer solutions. To ensure the proper establishment of steady state, the outflow at the column outlets was monitored during the course of experiments, and volumes of water in columns were determined by weighting before and after every experiment.

Nanoparticle BTCs and retention profiles

The monitoring of outlet concentration for bromide and NPs allowed the determination of breakthroughs curves (BTCs). NPs retention profiles were determined at the end of the experiment as follows. The columns were placed in the freezer for 12 h and then immersed in a warm tub of water at 60 °C in order to slide soil out from the columns and to cut slices around 2 cm thick. Each slice was homogenized and dried and 100 g were collected and placed in 200-mL plastic bottles to which 50 mL of water was added. The vials were agitated for 4 h using a mechanical mixer and supernatants were measured for fluorescence to determine NPs concentrations. It was assumed that all trapped NPs were removed by this process. The knowledge of the mass of entrapped colloids in liquid samples allowed the determination of the mass of NPs entrapped per gram of soil, i.e., of NPs retention profiles in the columns.

Moment method

The dynamics system approach was used to analyze tracer and NPs breakthrough curves. The input signal

was a pulse of either bromide solution or NPs solution with the same duration δt and concentrations of $C_{o,s} = 10^{-2}$ mol L^{-1} and $C_{o,p} = 0.2$ g L^{-1}. The breakthrough curves (BTCs) were first analyzed for their moments, these being defined as follows:

$$\mu_N = \int_0^{+\infty} \frac{C(t)}{C_0} t^N \mathrm{d}t \quad (5)$$

with $C(t)$ the concentration of bromide or NPs, C_0 the concentration injected at inlets, t time, and N the given order.

The mass balance (MB), corresponding to the ratio of the mass of solutes eluted over the mass injected, was calculated from the moment of order 0:

$$\mathrm{MB} = \frac{\mu_0}{\delta t} \quad (6)$$

The average residence time of NPs or bromide in the columns, t_s, corresponds to the average time spent by solutes in the columns. This time equals the mean time of solute elution minus the mean time necessary to enter the system, $\delta t/2$, and was computed from the moment of order 1:

$$t_s = \frac{\mu_1}{\mu_0} - \frac{\delta t}{2} \quad (7)$$

Theoretically, the solute mean residence time should correspond to the water residence time $t_{s,w}$, i.e., to the time needed to renew the water in the columns. The retardation factor evaluates the ratio of these two times:

$$R = \frac{t_s}{t_{s,w}} \quad (8)$$

$$t_{s,w} = \frac{L\,\theta}{q} \quad (9)$$

Mass balances and retardation factors permit to verify that the solute behaves as a tracer (with MB = 1 and $R = 1$), or if retention occurs (BM < 1 and $R > 1$) or if exclusion occurs ($R < 1$).

At last, the moment of order 2 allows the determination of BTCs variance σ^2 for assessing the degree of spreading around the mean:

$$\sigma^2 = \frac{\mu_2}{\mu_0} - \left(\frac{\mu_1}{\mu_0}\right)^2 \quad (10)$$

Bromide and nanoparticle transport models

After calculation of the experimental moments, experimental BTCs were fitted to transport models. The physical non-equilibrium transport model of fractionation of water in two phases, namely mobile and immobile water fractions, MIM, was chosen in this study given the asymmetrical shape of BTCs. For non-reactive solutes (tracer), transport in the mobile region combines convection, dispersion and solute exchange between mobile and immobile regions. Molecular diffusion is often neglected in both mobile and immobile water fractions assuming that convection and mechanical dispersion predominate. For steady state flow, the transfer equations for non-reactive solute (e.g., bromide) can be written as follows:

$$\theta_m \frac{\partial C_{m,s}}{\partial t} + \theta_{im} \frac{\partial C_{im,s}}{\partial t} = \lambda_s q \frac{\partial^2 C_{m,s}}{\partial z^2} - q \frac{\partial C_{m,s}}{\partial z} \quad (11)$$

with a first-order kinetics for solute exchange:

$$\theta_{im} \frac{\partial C_{im,s}}{\partial t} = \alpha_s \left(C_{m,s} - C_{im,s}\right) \quad (12)$$

where θ_m and θ_{im} are water contents occupied respectively by the mobile and immobile water fractions; λ_s (cm) is the dispersivity of the porous medium for the solute; α_s (min^{-1}) is the solute exchange coefficient. The fit of experimental data to MIM model provides the estimates for all hydrodynamic parameters: θ_m, θ_{im}, λ_s, and α_s. The analysis of these parameters allows the complete characterization of flow patterns in the columns. Several characteristic times allow the assessment of the relative influence of factors (water fractionation, limitation of solute diffusion at the interface between mobile and immobile fractions, etc.). Convection time t_m is the time taken by bromide or NPs to pass through the mobile water fraction. Mass transfer time t_α is the average exchange time between the mobile and immobile fractions (Hanna et al. 2012):

$$t_m = \frac{L\theta_m}{q} \quad (13)$$

$$t_\alpha = \frac{\theta_{im}}{\alpha_s} \quad (14)$$

where L (cm) is the length of the column.

For reactive solutes or particles and in particular NPs, physical processes (convection, dispersion and solute exchange at the interface mobile/immobile fractions) must be combined with the action of retention mechanisms. For a steady state flow, the NPs transfer equations can be written as follows:

$$\theta_m \frac{\partial C_{m,p}}{\partial t} + \theta_{im} \frac{\partial C_{im,p}}{\partial t} + f_{rac}\rho_d \frac{\partial S_{m,p}}{\partial t} + (1-f_{rac})\rho_d \frac{\partial S_{im,p}}{\partial t} = \lambda_p q \frac{\partial^2 C_{m,p}}{\partial z^2} - q \frac{\partial C_{m,p}}{\partial z} \quad (15)$$

$$\theta_{im} \frac{\partial C_{im,p}}{\partial t} + (1-f_{rac})\rho_d \frac{\partial S_{im,p}}{\partial t} = \alpha_p \left(C_{m,p} - C_{im,p}\right) \quad (16)$$

where f_{rac} is the fraction of sites in contact with mobile water; $C_{m,p}$ and $C_{im,p}$ (g L^{-1}) are the concentrations of NPs in the aqueous mobile and immobile phases, respectively; f_{rac} is the fraction of retention sites in contact with the mobile water; $S_{m,p}$ and $S_{im,p}$ (g g^{-1}) are the concentrations of NPs trapped into mobile and immobile water; λ_p (cm) is the dispersivity of the porous medium for NPs; and α_p (min^{-1}) is the exchange coefficient of NPs between mobile and immobile phases. The concentrations of entrapped NPs are related to concentrations in water using the attachment/detachment model (Šimůnek et al. 2008):

$$\rho_d \frac{\partial S_p}{\partial t} = \theta k_a C_p - k_d \rho_d S_p \quad (17)$$

where C_p (g L^{-1}) refers to the total resident concentration of NPs in liquid phase and S_p (g g^{-1}) the total sorbed concentration of NPs selected at time t. This model hypothesizes that NPs can be attached to the solid phase following a first-order kinetics (attachment coefficient k_a (min^{-1})) and detached following first-order kinetics (k_d detachment coefficient (min^{-1})). In a first attempt, values of coefficients k_a and k_d were similar in mobile and immobile water fractions.

Hydrus code for modeling transfer equations

The transfer of bromide and NPs was modeled using Hydrus 1D (Šimůnek et al. 2008). This program allows the numerical solving of flow and solute transfer equations for different initial conditions and under the limits of experiments on columns: known inlet concentration, zero gradient in concentration at the outlet, and no initial solute or NPs concentration. The estimation of transfer parameters is made by inverse modeling through fitting the calculated data to the experimental data and using the non-linear optimizing method of least squares based on the Levenberg-Marquardt algorithm (Marquardt 1963). When adjusting, the dispersivities (λ_s and λ_p) are considered as an intrinsic hydrodispersive characteristic of the soil (Bear 1972) and of the same order of magnitude as the largest grain size in the porous matrix. To model Eqs. 11, 12, 15, 16, and 17, the HYDRUS model was used as follows. Both physical non-equilibrium and chemical non-equilibrium options were selected in order to couple transport equation (15, 16) with a kinetically limited sorption (18):

$$\frac{\partial S_p}{\partial t} = \omega\left(K_d C_p - S_p\right) \quad (18)$$

where ω (min^{-1}) is the characteristic frequency of retention processes, K_d (g cm^{-3}) is the partition coefficient between the liquid and solid phases. Then, by identification of the terms of Eqs. 17 and 18, the relationship definition of coefficients k_a and k_d as a function of the parameters of Eq. 18 can easily be established leading to Eqs. 19 and 20. This approach is similar to work already done by several authors (e.g., Bradford et al. 2004; Pot et al. 2005; Gargiulo et al. 2007, 2008):

$$k_a = \frac{\omega \rho_d K_d}{\theta} \quad (19)$$

$$k_d = \omega \quad (20)$$

Results and discussions

Characterization of nanoparticles

Titration curves show similar trends with a decrease of zeta potential with pH for all ionic strengths (Fig. 3b).

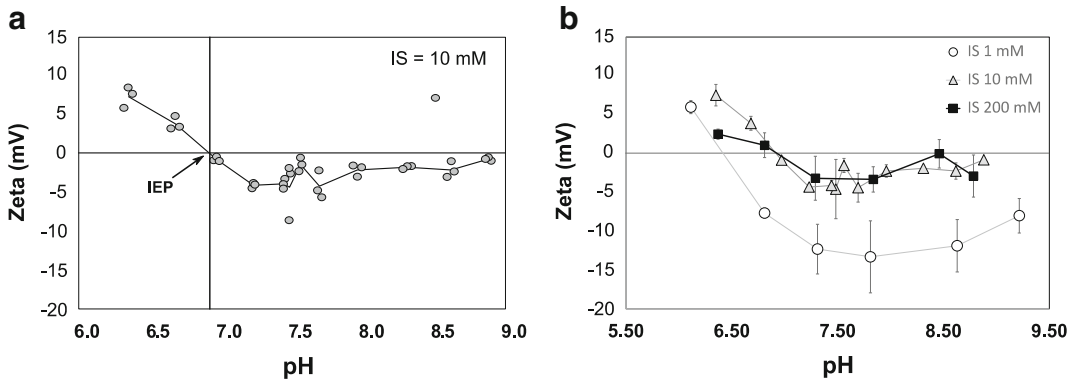

Fig. 3 Zeta potential as a function of pH at ionic strength (IS) = 10 mM (**a**) and for all ionic strengths (**b**). The ionic strength of 50 and 100 mM were not represented for clarity, means and standard deviations for **b**

For instance, at I_S = 10 mM, the titration curve shows a zeta potential around −5 mV in the alkaline range zone (pH >7) and between zero and 10 mV in the acid range (Fig. 3a). The increase in pH triggers the deprotonation of the NPs hydroxyl groups ($-OH \rightarrow -O^- + H^+$), and thus decreases the NPs surface charge. The pH of the isoelectric point (pH_{IEP}) is around 6.85. Similar results were obtained for the other ionic strengths, i.e., the NPs remain negatively charged at high values of pH and positively charged at low values of pH. pH_{IEP} is around 6.85 for I_S = 200 mM and drops down to 6.50 at I_S = 1 mM. For the lower ionic strength, the contrast in surface charge is stronger; the charges are less negative over the alkaline zone (pH >7). Among others, the NPs surface charge will influence their attachment to solid-water and air-water interfaces.

The apparent size of NPs was measured against pH (Fig. 4). The average size clearly depends on the value of pH whatever the ionic strength is (Fig. 4a). For all ionic strengths, the NPs average size reaches a maximum value around pH_{IEP}, i.e., pH_{IEP} ~6.5 for I_S = 1 mM and pH_{IEP} ~6.85 for $I_S \geq 10$ mM. The agglomeration of NPs is favored when the NPs surface charge is close to zero, i.e., close to the pH of the isoelectric point (pH_{IEP}). Above, the NPs average size exhibits a strong decrease down to the size of isolated NPs (around ~55 nm), indicating no agglomeration (Fig. 4a). This decrease occurs at a higher pH for higher I_S, revealing the positive effect of I_S on NPs agglomeration. Second positive effects of I_S: larger NPs agglomerates are obtained for higher values of I_S (≥10 mM), with a maximum size around 1200 nm. Such a size represents several dozen times the value of a single nanoparticle (~55 nm) and thus reveals the strong NPs agglomeration.

The analysis of the NPs average size is completed with the analysis of size distributions for the specific case of I_S = 10 mM (Fig. 4b–e). Based on NPs size distributions, five different statuses were defined from mono-dispersed state (S1) to agglomerated state (S5). These states are indicated in Fig. 4b as a function of pH for the specific case of I_S = 10 mM and related size distributions are depicted in Fig. 4c–e. The mono-dispersed solution (state S1) is encountered for high pH (>8.5) and includes mostly single particles with few large agglomerates (~4500 nm). For 7.2 < pH < 8.5, the agglomerate size increases and a third mode appears ranging from 450 to 1800 nm (Fig. 4d, states S2 to S4). For these cases, particle size distributions include three separate modes in varying proportions: one mode for isolated NPs, a second mode for agglomerates with a size from 55 to 1800 nm, and a third mode for larger agglomerates of 4500 nm (Fig. 4d, curves S3 and S4). Finally, when pH is close to pH_{IEP}, all NPs form agglomerates of two sizes, 1350 and 4500 nm (Fig. 4e). Clearly, NPs size distributions change with pH, allowing large to very large agglomerates to form at pH close to pH_{IEP}.

Potential for nanoparticle retention in the studied soil

DLVO calculations were performed to assess the likelihood of attachment to soil-water interface (SWI) and air-water interface (AWI). The zeta potential of the soil-solid particles was measured using a colloidal suspension of soil and averaged −4.75 mV over pH ranges 6–9. For the air-water interface, we considered the average value of −25 mV in agreement with the measures performed by Yang et al. (2001)on bubbles in water. For the NPs, given the titration curves obtained for all solutions

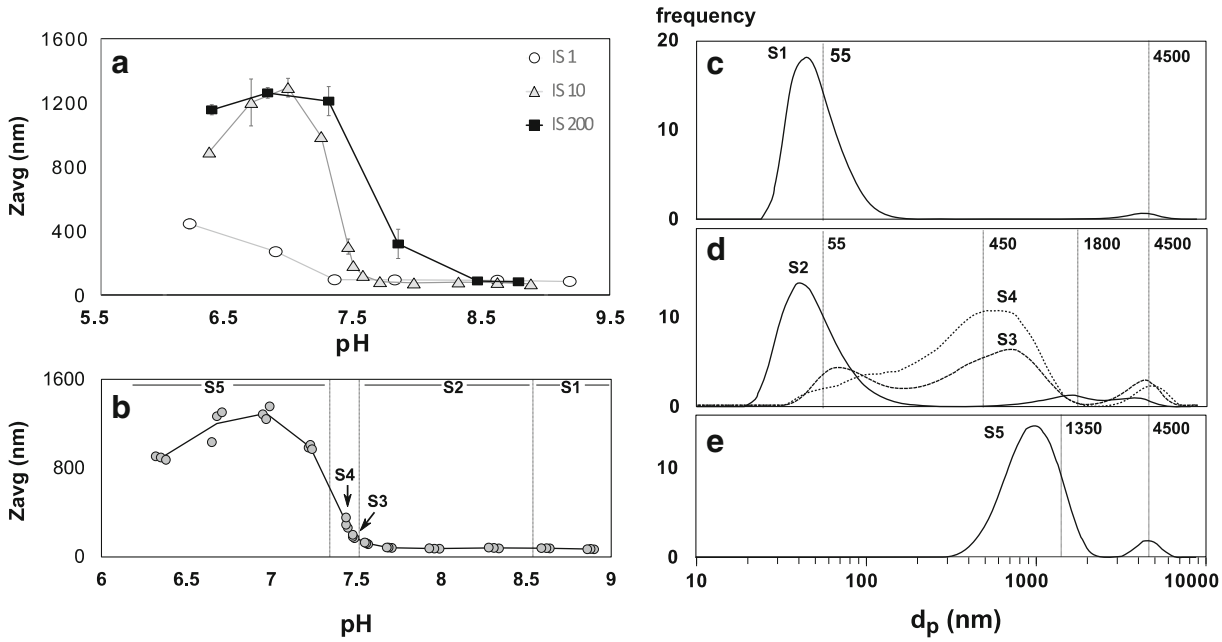

Fig. 4 Average size of particles (Zavg) as a function of pH for several ionic strengths (**a**), data in details at I_S = 10 mM and solution states from S1 to S5 (**b**), illustration of typical size distributions for every state from a solution S1 with mono-dispersed particles (**c**) to solution S5 made only of agglomerates (**e**), with transition states S2–S4 (**d**) at I_S = 10 mM (the frequency is plotted against the diameter of particles (d_p))

(Fig. 3), we considered two zones for pH: zeta ≈10 mV around pH = 6 and zeta ≈−10 mV around pH = 9. The calculated DLVO interaction energies in both sand-water-NP and air-water-NP are presented in Fig. 5 as a function of ionic strength and for pH = 6 and pH = 9. The DLVO interaction energies exhibit no high-energy barriers in all cases, showing favorable conditions for NPs attachment to SWI or AWI. It can be noted that at high pH for the AWI, small peaks appear (Fig. 5d) but they seem related to low values of energy. Briefly, DLVO calculations show that NPs attachment to soil-water and air-water interfaces are plausible in the studied porous medium over the pH ranges 6–9. Ionic strength does not change the DLVO interaction energies for attachment to SWI (Fig. 5a, c). Ionic strength removes the low-energy peak for AWI at pH = 9, thus favoring attachment to AWI at pH = 9 (Fig. 5d). However, its bulk effect on attachment to SWI and AWI should remain low.

The size of objects was compared to pore size distribution to assess the potential of straining in the studied soil. As suggested by Herzig et al. (1970), pores with sizes lower than 20 times the dimension of objects were hypothesized to participate in NPs entrapment. Considering such assumption, we calculated the threshold corresponding to 20 times the NPs average size for all states and reported these thresholds on the soil pore size distribution (Fig. 6a). We also calculated the volume percentages of pores of the porous medium smaller than these given thresholds (Fig. 6b). These data clearly show that pores are too large to trap lone NPs (S1) or NPs agglomerates formed at states S2 and S3. NPs entrapment slightly begins for state S4 and reaches its full potential at state S5. In this last case, close to 60% of pores may participate to entrapment. Similar conclusion may be stated for the other solutions since large objects can form for $I_S \geq 10$ mM (see Fig. 4). Clearly, the studied soil offer a potential for entrapment of NPs agglomerate and straining must be considered as a potential mechanism for NPs entrapment.

Effect of flow on transport of bromide and nanoparticles

Bromide BTCs are depicted in Fig. 7a. Bromide proved to be a good tracer with retardation factors, R, and mass balances, MB, around unity for the three flow rates studied. The missing 4% for mass balance (Table 1) can be explained by underestimation of the concentrations at the column outlets. Tracer BTCs were well described by the MIM model, with accurate fits (Fig. 7a) and regression

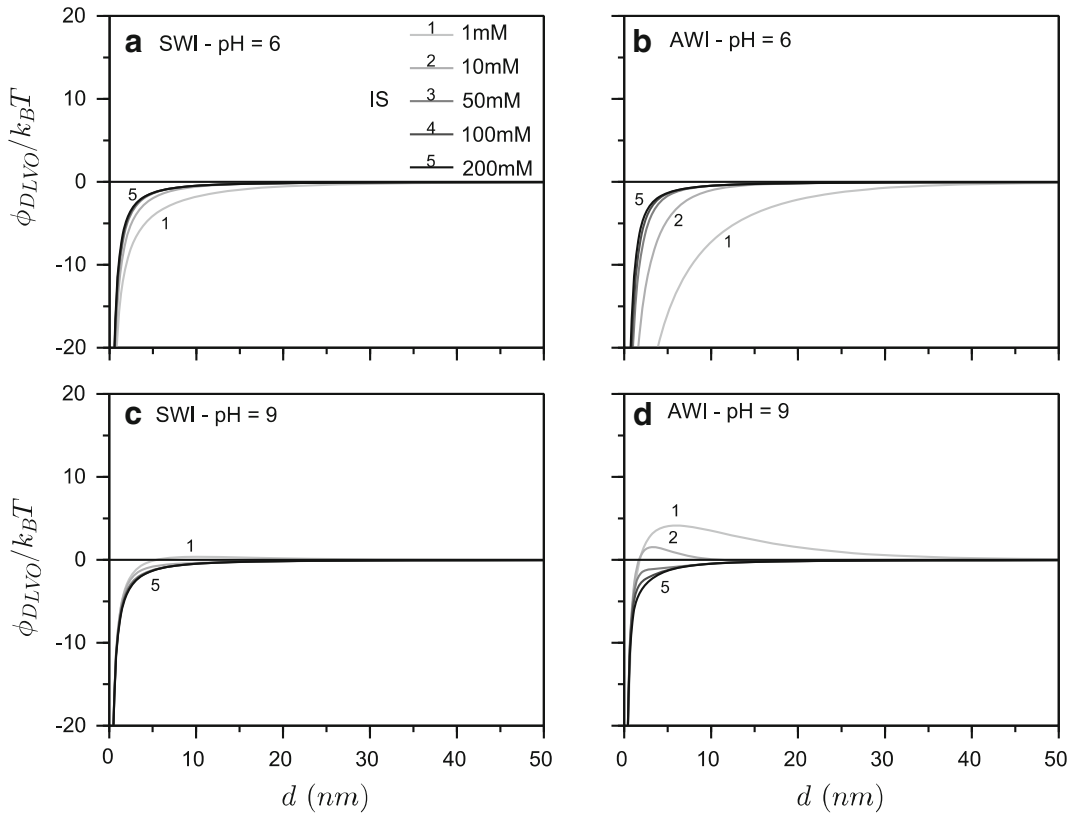

Fig. 5 DLVO calculations at the soil-water interface (SWI) and air-water interface (AWI) as a function of ionic strength and for two contrasting values of pH (6 and 9); the total potential $\varnothing_{DLVO}/k_BT$ is plotted against the distance between particles d

coefficients >0.99 in all cases. Asymmetrical shapes of BTCs are typical for dispersive flow and water fractionation into mobile and immobile water contents, which is confirmed by hydrodispersive parameters listed in Table 1.

Bromide dispersivity increases when flow rate decreases (Table 1), which has already been discovered and linked to the decrease in water content of unsaturated materials (Torkzaban et al. 2006b; Toride et al. 2003). For the specific case of this study, volumetric water

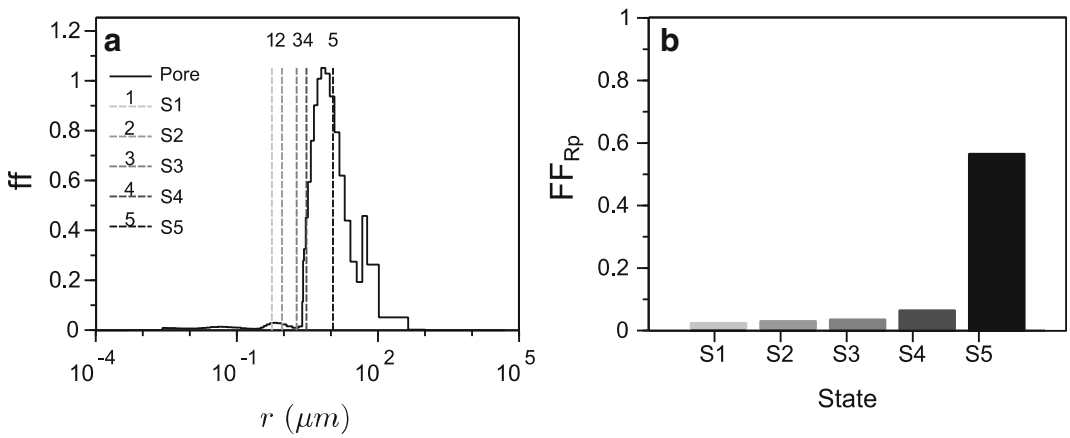

Fig. 6 Pore size distribution of the studied medium (the frequency *ff* is plotted against the particle radius *r*) and sizes of pores capable of retention of NPs agglomerates with state averaged diameters (*dashed lines*) (a); corresponding percentages of pores allowing retention in the porous medium (FF_{Rp}) as a function of the solution states (S1–S5) (b)

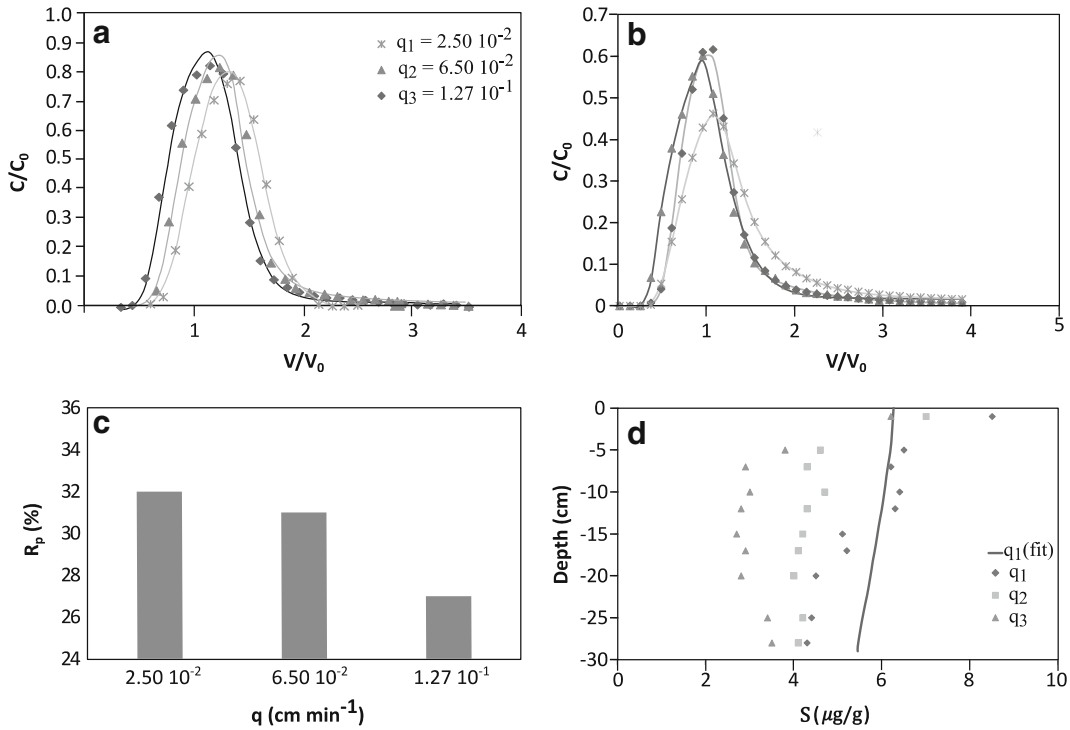

Fig. 7 Effect of velocity on transfer at I_S = 10 mM. Bromide breakthrough curves (**a**), NPs breakthrough curves (**b**), NPs retention at column scale R_p (**c**), and NPs retention profiles (**d**) measures (*symbols*) and modeled data (*solid lines*). C/C_0 relative concentration, V/V_0 pore volume, S concentration of retained NPs, R_p fraction of NPs retained in the columns

content decreased from 0.21 to 0.14 $cm^3\ cm^{-3}$ with the decrease of flow rate. Lower water contents means more air in the pore space, which increases the complexity and the tortuosity of flow pathways leading to more dispersion for solutes and particles carried by water (Padilla et al. 1999; Torkzaban et al. 2008; Lamy et al. 2013). The flow is more homogenous at low flow rate. Mobile fraction, f_m, increases from 55 to 86% when flow rate is decreased from 0.127 to 0.025 cm min^{-1} (Table 1). Characteristic exchange time between mobile and immobile waters, t_α, is lower at low flow rate (Table 1), revealing a more rapid and efficient solute exchange between mobile and immobile water fractions. For the higher flow rates, t_α is 10 times higher than convection time t_m (Table 1), revealing a strong limitation of solute exchange between mobile and immobile water fractions. In this case, immobile water fraction is not easily accessible to solutes. Such dependency of flow pattern on flow rate have already been found by previous authors (e.g., Padilla et al. 1999; Lamy et al. 2013; Prédélus et al. 2014).

For all flow rates, NPs exhibit bell-shaped BTCs, as bromide, but with lower peaks and more asymmetrical shapes (Fig. 7b versus 7a). Lower peaks indicate a significant retention of NPs in the columns. Mass balance factors, MB_p, and percentages of NPs retained in the columns, $R_p = 1 - MB_p$, confirmed this statement. Around 30% of injected NPs were retained in the columns, and retention decreased when flow rate increased (Fig. 7c). Regardless of flow rate, nanoparticles were

Table 1 Hydrodispersive bromide parameters for the three flow rates at I_S = 10 mM

q (cm min^{-1})	MB (%)	λ_s (cm)	α_s (min^{-1})	f_m (%)	t_s (min)	t_m (min)	t_α (min)
0.025	96	0.9	$1.6\ 10^{-4}$	86	147	124	108
0.065	96	0.8	$2.5\ 10^{-4}$	76	89	68	180
0.127	97	0.7	$3.4\ 10^{-4}$	55	47	26	261

mostly retained at the column inlet (i.e., between 0 and 5 cm depth) as shown by NPs retention profiles (Fig. 7d). Regarding the comparison between flow rates, NPs retention is lowered over the whole profile when flow rate is increased (Fig. 7d).

The MIM model coupled with the attachment/detachment model (Eqs. 15–17) properly fits NPs experimental BTCs (Fig. 7b). Yet, the fit was less accurate for NPs retention profiles, as illustrated for the case of the lowest flow rate (Fig. 7d). The values of hydrodispersive parameters derived from tracer experiments could not be used directly for NPs and had to be optimized specifically. As frequently found, NPs and water do not follow the same pathways (e.g., Bradford et al. 2003). The optimized values of hydrodispersive parameters show the dependency of pathways followed by NPs upon flow rates (Table 2). Briefly, they suggest that the transfer of NPs is more homogeneous at a low flow rate as for flow. For instance, the mobile water fractions visited by NPs scores 96% against 59% when comparing the lowest rate to the highest flow rate (Table 2). The analysis of attachment and detachment coefficients k_a and k_d and fraction of retention sites in contact with mobile water f_{rac} gives further information about retention. Retention of the NPs can be regarded as reversible when $k_d/k_a = 1$. In this work, k_d/k_a values range between 0.025 for the largest flow rate and 0.19 for the smallest flow rate (Table 2). The values of k_a, k_d, and k_d/k_a confirm that retention is more important and more reversible at a low flow rate. Lastly, the values of the fraction of sorption sites in contact with mobile water are similar to the mobile water fraction, $f_{rac} \approx f_m$ (Table 2), indicating no preferential entrapment of NPs in one of the mobile/immobile water fractions (Šimůnek and van Genuchten 2008).

As detailed above, NPs retention in the water-unsaturated columns may result from the concomitancy of several complex mechanisms: attachment onto solid-water (SWI) or air-water interface (AWI); bridging, wedging or straining; film straining; and coagulation or agglomeration (Mitropoulou et al. 2013). As detailed above, DLVO calculations show that NPs may be retained by attachment to SWI or AWI for any pH between 6 and 9. Such pH range is highly plausible in the studied soil, given its high carbonate content (Lassabatere et al. 2004, 2007). Indeed, NPs solutions enter columns at a pH around 6.5. Due to the high carbonate content, pH may increase up to values between 7.5 and 8.5 depending on flow rate (Lassabatere et al. 2007). In addition, NPs retention by straining is also plausible. Indeed, the section above clearly demonstrated that NPs may agglomerate to form objects of several hundred or even several thousand nanometers, these being easily trapped by soil pores. However, agglomeration requires state S5 of the interstitial water, meaning a value of pH close to pH_{IEP} with $pH_{IEP} \approx 6.5$ for $I_S = 1$ mM and $pH_{IEP} \approx 6.85$ for $I_S \geq 10$ mM. As detailed above, pH increases from column inlets to outlets and moves apart from pH_{IEP} with depth. Consequently, NPs agglomeration and entrapment of NPs agglomerates by straining should be more efficient close to column inlets. These hypotheses are consistent with the large drop in NPs retention close to column inlets as revealed by experimental retention profiles (Fig. 7d). Briefly, NPs retention in the columns may result from the combination of entrapment of NPs agglomerates by straining close to column inlets and attachment to SWI and AWI along the whole columns.

The decrease in global NPs retention with the increase of flow rate may result from several flow factors. At first, any change in flow rate may affect flow velocity at a pore scale. Bradford et al. (2007) observed that any increase in water velocity increases the magnitude of the lift and drag forces acting on colloids near solid surfaces, and thus inhibits particle retention. Clearly, water velocity increase may have a negative impact on straining and attachment to SWI and AWI as well. Yet, not only flow rate but also the homogeneity of flow may play a significant role (Šimůnek and van Genuchten 2008). When flow is heterogeneous, preferential flow pathways may establish and carry NPs in fast flow zones away from sorption sites. On the other hand, a more homogeneous flow may

Table 2 Hydrodispersive and retention parameters of NPs for the three flow rates at $I_S = 10$ mM

q (cm min^{-1})	MB (%)	λ_p (cm)	f_m (%)	f_{rac} (%)	α_p (min^{-1})	k_d (min^{-1})	k_a (min^{-1})	k_d/k_a (−)
0.025	68	0.8	96	84	$4.3\ 10^{-4}$	$1.2\ 10^{-3}$	$6.3\ 10^{-3}$	0.19
0.065	69	0.7	67	75	$4.3\ 10^{-3}$	$4.2\ 10^{-4}$	$2.6\ 10^{-3}$	0.16
0.127	73	1.1	59	60	$3.7\ 10^{-3}$	$5.0\ 10^{-4}$	$2.0\ 10^{-2}$	0.025

prevent the establishment of preferential flow pathways and increase the likelihood of NPs coming into contact with sorption sites as already suggested for solutes (Lassabatere et al. 2004, 2007; Lamy et al. 2009; Lamy et al. 2013). In this study, homogeneous flow was observed for the lowest flow rate, which could explain to a certain extent the better retention of NPs. Another physical side effect of flow rate is the water content in the porous medium. As mentioned above, water content decreases for lower flow rates, leading to an increase in the surfaces of air-water interfaces and thus NPs entrapment by film straining or attachment to AWI (Torkzaban et al. 2006a, b, 2008).

These flow factors are combined with physicochemical effects. Flow rate and flow homogeneity impact the pH by ruling the contact between calcareous grains and interstitial water. Lower flow rates and more homogeneous flow may ease the dissolution of calcite and thus favor the increase in pH (Lassabatere et al. 2007). This in turn may have a negative effect on NPs agglomeration and entrapment on NPs agglomerate by straining (see Fig. 4b). Consequently, such conditions should reduce NPs retention by straining. As opposed to straining, attachment to SWI and AWI are not significantly impacted by pH (see DLVO calculations). As mentioned above, whatever the value of pH, no high-energy peak appears and prevents from attachment to SWI and AWI. Yet, no specific geochemical effect is expected on NPs attachment to SWI and AWI. These hypotheses are consistent with retention profiles (Fig. 7d). Indeed, for the lowest flow rate, retention decreases less over soil profile, indicating less removal by NPs agglomeration and entrapment of agglomerates. At the opposite, the highest velocity exhibit a large decrease in retention profile, which can be interpreted as significant retention by NPs agglomeration and entrapment of agglomerates close to the column inlet. This difference could result from less NPs agglomeration and entrapment of agglomerates by straining due to a higher pH in columns submitted to the lowest flow rate. Finally, regarding physicochemical effects, the lower velocity should be less favorable to NPs overall retention due to its negative effect on NPs agglomeration. Finally, the effect of the decrease in flow rate may result from two antagonist effects, i.e., positive physical flow factors (homogenization of flow and lower flow rates) and negative physicochemical factors (higher pH along the column). Experimental data show that the global effect is positive.

Effect of ionic strength on nanoparticle retention

NPs breakthrough elution curves (BTCs) are depicted for the different ionic strengths along with modeled data in Fig. 8a. Flow rate was fixed at the highest velocity (0.127 cm min^{-1}) and flow in the columns was already described as fractionated into mobile and immobile water fractions. For all ionic strengths, the BTCs show no delay in comparison to the tracer with a breakthrough around one pore volume. NPs show more dispersion and asymmetry for the cases of I_S = 10 mM and I_S = 50 mM. For the latter, the smaller magnitude of the peak results from the efficiency of NPs retention in the systems. The percentage of NPs retained in the columns, R_p, shows the influence of ionic strength on NPs retention (Fig. 8b). Clearly, the influence of ionic strength splits into two distinct parts. For ionic strengths between 1 and 50 mM, NPs retention increases with ionic strength (Fig. 8b). Above 50 mM, the increase in ionic strength produces a reversal in trend (Fig. 8b). Such reversal has scarcely been found, even if quite significant in this study: NPs retention scores around ~45% for I_S = 50 mM and decreases down to ~20% for I_s = 100 mM before increasing again up to ~30% for I_S = 200 mM. Obviously, an optimal retention is obtained at an ionic strength of 50 mM.

The analysis of attachment and detachment coefficients obtained by inverse modeling (Table 3) gives further information about the evolution of global retention R_p. Between 1 and 50 mM, detachment remains roughly constant (Fig. 8c), whereas the attachment coefficient increases (Fig. 8d). The global increase in retention may result mainly from the increase in attachment or retention mechanisms. On the contrary, between I_S = 50 mM and I_S = 100 mM, the attachment coefficient decreases while the detachment coefficient increases sharply (Fig. 8c). When ionic strength increases up to 200 mM, detachment decreases again (Fig. 8c) with quite stable values for attachment coefficients (Fig. 8d). Briefly, the reversal in global NPs retention between 50 and 100 mM may result from a more significant detachment of NPs or agglomerates. This statement results exclusively from the analysis of model parameters and thus should be confirmed by additional data and observations. Yet, model parameters and significant values of detachment coefficients are in

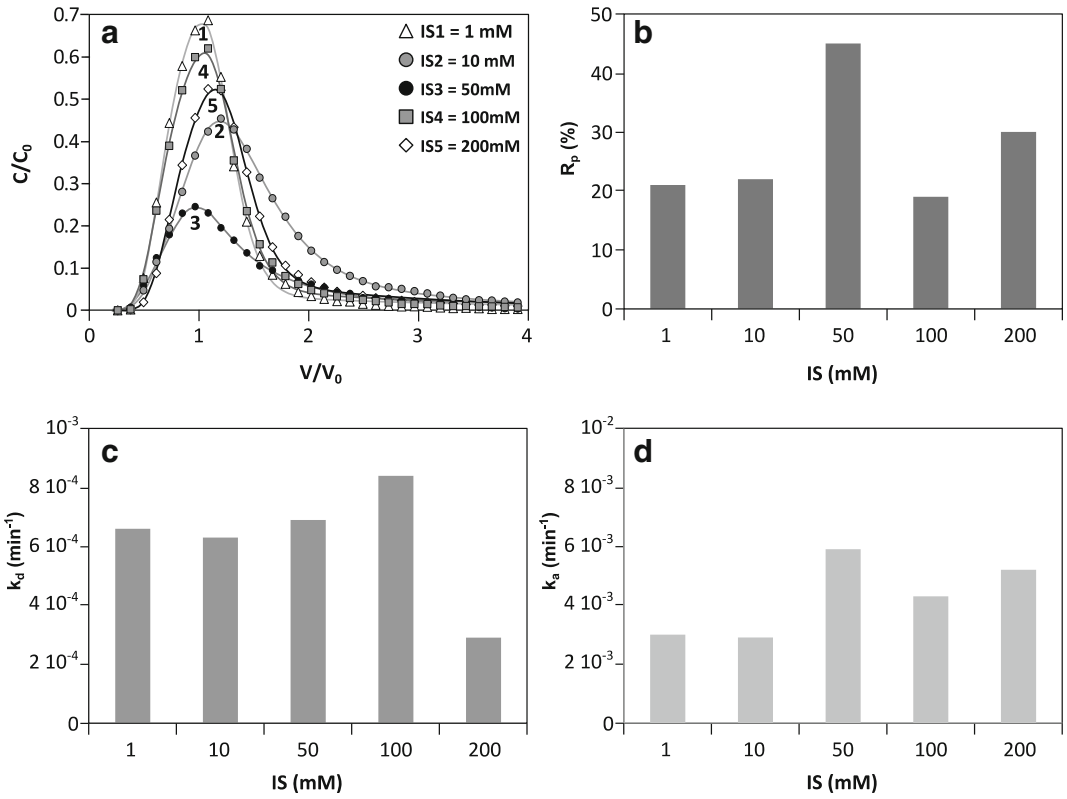

Fig. 8 Influence of ionic strength on transfer. Measured (*symbols*) and simulated (*lines*) breakthrough curves of nanoparticles for the five ionic strengths at q = 0.127 cm min^{-1}(**a**), global retention at column scale, R_p, as a function of ionic strength (**b**), attachment and detachment coefficients, k_a and k_d, as a function of ionic strength, I_S (**c**–**d**)

line with experimental BTCs and particularly the tails observed for some of them (Fig. 8a). These tails may indicate that some of the NPs retained in the columns may finally manage to escape later.

The increase in NPs retention with ionic strength has been reported in literature many times (e.g., Compère et al. 2001; Redman et al. 2004; Rousseau et al. 2004; Jacobs et al. 2007; Majdalani et al. 2007; Chowdhury et al. 2011; Fang et al. 2013). However, Mitropoulou et al. (2013) observed a slight decrease in retention for spherical polymer microspheres (300 μm in diameter) in quartz sand, when increasing ionic strength from 5 mM to 50 or to 100 mM. However, this decrease in NPs retention was much smaller than that observed in this study. Ionic strength of solution facilitates the agglomeration of NPs by reducing the thickness of the double layer of NPs. Enhancement of NPs agglomeration should facilitate their retention due to the entrapment of NPs agglomerates by straining. This was clearly observed for the studied NPs (Fig. 5) with an increase in agglomeration with ionic strength. For attachment to SWI, DLVO calculations clearly demonstrate that

Table 3 Hydrodispersive and retention parameters of NPs for the five ionic strengths at q = 0.127 cm min^{-1}

I_S (mM)	MB (%)	λ_p (cm)	f_m (%)	α_p (min^{-1})	k_d (min^{-1})	k_a (min^{-1})	k_d/k_a (%)
1	79	1.1	66.0	5.6 10^{-4}	6.6 10^{-4}	3.0 10^{-3}	0.22
10	78	3.0	87.5	8.8 10^{-4}	6.3 10^{-4}	2.9 10^{-3}	0.21
50	55	0.7	61.0	5.9 10^{-3}	6.9 10^{-4}	5.9 10^{-3}	0.11
100	81	1.4	59.5	7.2 10^{-4}	8.4 10^{-4}	4.3 10^{-3}	0.19
200	70	1.1	65.0	9.8 10^{-4}	2.9 10^{-4}	5.2 10^{-3}	0.05

attraction should be mostly unchanged (Fig. 5a, c), except for attachment to AWI, with a potential slight increase at pH 9 (Fig. 5d). Regardless the involved retention mechanism (sorption to SWI or AWI or NPs agglomeration and entrapment of agglomerates by straining), ionic strength should favor NPs retention at the column scale.

There is no clear explanation for the reversal observed in NPs retention (Fig. 8d). Ionic strength should promote NPs retention. In addition, the range of pH in the columns should not change significantly between the five ionic strengths. Indeed, ionic strength is not expected to influence calcite dissolution and, in turn, pH (Appelo and Postma 2004). The reversal of retention is not a question of pH and may be explained by a combination of complex mechanisms. The combination of physical (straining), physicochemical (NPs agglomeration, attachment to SWI and AWI), and geochemical mechanisms (effect of pH, composition of the interstitial water) should be investigated more deeply. Complex geochemical processes are known to rule the fate of colloids or nanoparticles (Torkzaban et al. 2012). For the specific case of this study, we accounted for the effect of calcite dissolution on pH and in turn on NPs retention, but we should also investigate additional effects. Indeed, calcite dissolution may bring calcium and magnesium, two divalent ions that may play specific roles with regards to attraction/repulsion forces. In addition, cationic exchange and surface complexation may also occur (Lassabatere et al. 2007), thus promoting the exchange between divalent and monovalent ions and changing the composition of interstitial water. Cationic exchange and surface complexation are highly sensitive to ionic strength (Appelo and Postma 2004). These aspects should require deeper geochemical modeling and coupling with the modeling of NPs transfer. Physical aspects require to be further investigated as well. The potential changes in pore network with straining should be accounted for. In fact, retained NPs agglomerates can block pores and change the network of pores active for flow. The transfer of non-agglomerated NPs may be shifted to regions with more open flow where electrostatic adhesion is less important, which may in turn reduce their retention. Higher I_S may eventually favor NPs agglomeration and deposition pattern to the point of a drastic change in pore structure, thus changing flow pathways and local hydrodynamics and thus disfavoring NPs retention. These hypotheses should be investigated more deeply.

Conclusion

In this study, the effect of flow and ionic strength of the solution on NPs retention was investigated in an unsaturated calcareous soil. The studied NPs were grafted with fluorescein derivatives to allow measurement of retained NPs concentrations even at very low concentrations and allowed the full determination of retention profiles. Indeed, previous studies have highlighted the difficulty of determining such profiles (Lamy et al. 2010, 2013), whereas these are known to be necessary for the identification of retention mechanisms (Bradford and Bettahar 2006). DLVO calculations showed the potential for NPs sorption to SWI and AWI in the studied soils. Particle size distribution shows the potential for NPs agglomeration with sizes large enough to allow entrapment by straining. These last phenomena seem much more sensitive to pH and ionic strength.

The leaching column experiments were performed with five ionic strengths and three different flow rates. Bromide was used to map flow in columns and NPs profile retention and breakthrough curves were determined. Bromide and NPs elution curves were well described by the MIM model (mobile-immobile) and allowed the following statements. Decreasing flow rate led to an increase in NPs retention. This effect was related to several potential effects: homogenization of flow, decrease in pore water velocity and in drag and lift forces, increase in air content, and attachment to AWI. Some geochemical effects are also suspected with an impact of flow rate on calcite dissolution and in turn on NPs agglomeration and entrapment by straining. The results showed that ionic strength plays an important role in mechanisms of transport and retention of NPs. Retention increases with the ionic strength of the solution (1, 10, and 50 mM); however, with an ionic strength above 50 mM (i.e., 100 and 200 mM), an opposite trend appears with a decrease in NPs retention. Such reversal has scarcely been observed and need further investigations to be explained. Geochemistry may play a role particularly in regards to NPs agglomeration or attachment to SWI and AWI. Further investigations may be conducted to perform a complete geochemical modeling and to account for additional mechanisms like pore structure evolution and its consequences on flow, NPs retention, and transfer.

This paper shows that the mechanisms responsible for NPs transfer in the environment are complex and interfere with both physical mechanisms (flow) and

complex geochemical processes. These must be accounted for if the understanding of the fate of NPs is targeted. In particular, flow and its homogeneity must be properly characterized and modeled because of their influence on retention mechanisms. Geochemistry must also be properly understood in terms of bulk parameters (pH and ionic strength) as well as in terms of composition of interstitial water. A full description of geochemical mechanisms must be performed to allow the understanding of mechanisms responsible for NPs retention in soils and their fate in the environment. At last, this paper presents a first step towards the comprehension of the fate of these NPs in the environment by presenting 1D leaching column experiments. In the field, soils and vadose zone are far from being homogeneous and 1D column experiments should be combined with additional measurements, observations, and laboratory experiments. For this purpose, a specific lysimeter was developed to mimic a heterogeneous vadose zone, and the study of the fate of the same NPs showed the tremendous effect of vadose zone heterogeneity on the fate of NPs (Prédélus et al. 2015). The advantage of investigations across scale is clearly stated.

Acknowledgements The authors are grateful to the OTHU, Greater Lyon and the ANR-GESSOL program (FAFF project: Filtration Function of an Urban Structure—Consequence on the Formation of an Anthroposol) for their logistic and financial support.

Compliance with ethical standards The authors declare that they have no conflict of interest.

References

Appelo CAJ, Postma D (2004) Geochemistry, groundwater and pollution. CRC press, New York **634 p**

Arya LM, Paris JF (1981) A physico-empirical model to predict the soil moisture characteristic from particle-size distribution and bulk density data. Soil Sci Soc Am J 45:1023–1030

Bear J (1972) Dynamics of fluids in porous media. American Elsevie Publishing Company, New York **764 p**

Bradford SA, Bettahar M (2006) Concentration dependent transport of colloids in saturated porous media. J Contam Hydrol 82:99–117

Bradford SA, Bettahar M, Simunek J, Van Genuchten MT (2004) Straining and attachment of colloids in physically heterogeneous porous media. Vadose Zone J 3:384–394

Bradford SA, Torkzaban S (2008) Colloid transport and retention in unsaturated porous media: a review of interface-, collector-, and pore-scale processes and models. Vadose Zone J 7: 667–681. doi:10.2136/vzj2007.0092

Bradford SA, Simunek J, Bettahar M et al (2003) Modeling colloid attachment, straining, and exclusion in saturated porous media. Environ Sci Technol 37:2242–2250

Bradford SA, Torkzaban S, Walker SL (2007) Coupling of physical and chemical mechanisms of colloid straining in saturated porous media. Water Res 41:3012–3024

Chen L, Sabatini DA, Kibbey TC (2008a) Role of the air–water interface in the retention of TiO2 nanoparticles in porous media during primary drainage. Environ Sci Technol 42: 1916–1921

Chowdhury I, Hong Y, Honda RJ, Walker SL (2011) Mechanisms of TiO2 nanoparticle transport in porous media: role of solution chemistry, nanoparticle concentration, and flowrate. J Colloid Interface Sci 360:548–555

Chen L, Sabatini DA, Kibbey TCG (2008b) Role of the air–water interface in the retention of TiO2 nanoparticles in porous media during primary drainage. Env Sci Tech 42:1916–1921

Compère F, Porel G, Delay F (2001) Transport and retention of clay particles in saturated porous media. Influence of ionic strength and pore velocity J Contam Hydrol 49:1–21

DeNovio NM, Saiers JE, Ryan JN (2004) Colloid movement in unsaturated porous media. Vadose Zone J 3:338–351

Derjaguin B, Landau L (1941) Theory of the stability of strongly charged lyophobic sols and of the adhesion of strongly charged particles in solutions of electrolytes. Acta Physicochim URSS 14:633–662

Fang J, Xu M, Wang D et al (2013) Modeling the transport of TiO2 nanoparticle aggregates in saturated and unsaturated granular media: effects of ionic strength and pH. Water Res 47:1399–1408

Gargiulo G, Bradford S, Simunek J et al (2008) Bacteria transport and deposition under unsaturated flow conditions: the role of water content and bacteria surface hydrophobicity. Vadose Zone J 7:406–419

Gargiulo G, Bradford S, Šimůnek J et al (2007) Bacteria transport and deposition under unsaturated conditions: the role of the matrix grain size and the bacteria surface protein. J Contam Hydrol 92:255–273

Goutaland D, Winiarski T, Dubé J-S et al (2008) Hydrostratigraphic characterization of glaciofluvial deposits underlying an infiltration basin using ground penetrating radar. Vadose Zone J 7:194–207

Grolimund D, Elimelech M, Borkovec M et al (1998) Transport of in situ mobilized colloidal particles in packed soil columns. Environ Sci Technol 32:3562–3569

Hanna K, Rusch B, Lassabatere L et al (2010) Reactive transport of gentisic acid in a hematite-coated sand column: experimental study and modeling. Geochim Cosmochim Acta 74: 3351–3366

Hanna K, Lassabatere L, Bechet B (2012) Transport of two naphthoic acids and salicylic acid in soil: experimental study and empirical modeling. Water Res 46:4457–4467

Herzig J, Leclerc D, Goff PL (1970) Flow of suspensions through porous media—application to deep filtration. Ind Eng Chem 62:8–35

Jacobs A, Lafolie F, Herry J, Debroux M (2007) Kinetic adhesion of bacterial cells to sand: cell surface properties and adhesion rate. Colloids Surf B Biointerfaces 59:35–45

Johnson WP, Tong M, Li X (2007) On colloid retention in saturated porous media in the presence of energy barriers: the failure of α, and opportunities to predict η. Water Resour Res 43

Keller AA, Auset M (2007) A review of visualization techniques of biocolloid transport processes at the pore scale under saturated and unsaturated conditions. Adv Water Resour 30: 1392–1407

Kretzschmar R, Borkovec M, Grolimund D, Elimelech M (1999) Mobile subsurface colloids and their role in contaminant transport. Adv Agron 121–193

Lamy E, Lassabatere L, Bechet B, Andrieu H (2013) Effect of a nonwoven geotextile on solute and colloid transport in porous media under both saturated and unsaturated conditions. Geotext Geomembr 36:55–65. doi:10.1016/j.geotexmem.2012.10.009

Lamy E, Lassabatere L, Bechet B, Andrieu H (2010) Flow and colloidal transfer in a dual porosity medium. Houille Blanche-Rev Int Eau 86–92

Lamy E, Lassabatere L, Béchet B, Andrieu H (2009) Modeling the influence of an artificial macropore in sandy columns on flow and solute transfer. J Hydrol 376:392–402

Lassabatere L, Spadini L, Delolme C et al (2007) Concomitant Zn-Cd and Pb retention in a carbonated fluvio-glacial deposit under both static and dynamic conditions. Chemosphere 69: 1499–1508. doi:10.1016/j.chemosphere.2007.04.053

Lassabatere L, Winiarski T, Galvez-Cloutier R (2004) Retention of three heavy metals (Zn, Pb, and Cd) in a calcareous soil controlled by the modification of flow with geotextiles. Environ Sci Technol 38:4215–4221. doi:10.1021/es035029s

McGechan M, Lewis D (2002) SW—soil and water: transport of particulate and colloid-sorbed contaminants through soil, part 1: general principles. Biosyst Eng 83:255–273

Marquardt DW (1963) An algorithm for least-squares estimation of nonlinear parameters. SIAM J Appl Math 11:431–441

Majdalani S, Michel E, Di Pietro L, Angulo-Jaramillo R, Rousseau M (2007) Mobilization and preferential transport of soil particles during infiltration: a core-scale modeling approach. Water Resour. Res. 43

Mitropoulou PN, Syngouna VI, Chrysikopoulos CV (2013) Transport of colloids in unsaturated packed columns: role of ionic strength and sand grain size. Chem Eng J 232:237–248

Padilla IY, Yeh T-CJ, Conklin MH (1999) The effect of water content on solute transport in unsaturated porous media. Water Resour Res 35:3303–3313

Pot V, Šimůnek J, Benoit P et al (2005) Impact of rainfall intensity on the transport of two herbicides in undisturbed grassed filter strip soil cores. J Contam Hydrol 81:63–88

Powelson DK, Gerba CP, Yahya MT (1993) Virus transport and removal in wastewater during aquifer recharge. Water Res 27:583–590

Prédélus D, Lassabatere L, Coutinho A et al (2014) Tracing water flow and colloidal particles transfer in an unsaturated soil. J Water Resour Prot 6:696–709

Prédélus D, Coutinho AP, Lassabatere L et al (2015) Combined effect of capillary barrier and layered slope on water, solute and nanoparticle transfer in an unsaturated soil at lysimeter scale. J Contam Hydrol 181:69–81. doi:10.1016/j.jconhyd.2015.06.008

Redman JA, Walker SL, Elimelech M (2004) Bacterial adhesion and transport in porous media: role of the secondary energy minimum. Environ Sci Technol 38:1777–1785

Rousseau M, Di Pietro L, Angulo-Jaramillo R, Tessier D, Cabibel B (2004) Preferential transport of soil colloidal particles: physicochemical effects on particle mobilization. Vadose Zone J 3:247–261

Ruckenstein E, Prieve DC (1976) Adsorption and desorption of particles and their chromatographic separation. AICHE J 22: 276–283. doi:10.1002/aic.690220209

Ryan J, Illangasekare T, Litaor M, Shannon R (1998) Particle and plutonium mobilization in macroporous soils during rainfall simulations. Environ Sci Technol 32:476–482

Sirivithayapakorn S, Keller A (2003) Transport of colloids in saturated porous media: a pore-scale observation of the size exclusion effect and colloid acceleration. Water Resour Res 39

Šimůnek J, van Genuchten MT (2008) Modeling nonequilibrium flow and transport processes using HYDRUS. Vadose Zone J 7:782–797

Šimůnek J, van Genuchten MT, Sejna M (2008) Development and applications of the HYDRUS and STANMOD software packages and related codes. Vadose Zone J 7:587–600

Solovitch N, Labille J, Rose J et al (2010) Concurrent aggregation and deposition of TiO2 nanoparticles in a sandy porous media. Environ Sci Technol 44:4897–4902

Tian Y, Gao B, Wang Y et al (2012) Deposition and transport of functionalized carbon nanotubes in water-saturated sand columns. J Hazard Mater 213–214:265–272

Torkzaban S, Bradford SA, van Genuchten MT, Walker SL (2008) Colloid transport in unsaturated porous media: the role of water content and ionic strength on particle straining. J Contam Hydrol 96:113–127

Torkzaban S, Hassanizadeh S, Schijven J, Van Den Berg H (2006a) Role of air-water interfaces on retention of viruses under unsaturated conditions. Water Resour Res 42(12)

Torkzaban S, Wan J, Tokunaga TK, Bradford SA (2012) Impacts of bridging complexation on the transport of surface-modified nanoparticles in saturated sand. J Contam Hydrol 136–137:86–95

Torkzaban S, Hassanizadeh S, Schijven J, de Bruin HAM, de Roda Husman AM (2006b) Virus transport in saturated and unsaturated sand columns. Vadose Zone J 5:877–885

Toride N, Inoue M, Leij FJ (2003) Hydrodynamic dispersion in an unsaturated dune sand. Soil Sci Soc Am J 67:703–712

Verwey E, Overbeek JTG (1955) Theory of the stability of lyophobic colloids. J Colloid Sci 10:224–225

Wan J, Wilson JL (1994) Visualization of the role of the gas-water interface on the fate and transport of colloids in porous media. Water Resour Res 30:11–24

Winiarski T, Lassabatere L, Angulo-Jaramillo R, Goutaland D (2013) Characterization of the heterogeneous flow and pollutant transfer in the unsaturated zone in the fluvio-glacial deposit. Procedia Environ Sci 19:955–964. doi:10.1016/j.proenv.2013.06.105

Yang C, Dabros T, Li D, Czarnecki F, Masliyah JH (2001) Measurement of the zeta potential of gas bubbles in aqueous solutions by microelectrophoresis method. J Colloid Interface Sci 243:128–135

Zang D, Zhang Y, Hou Q (2012) Effect of hydrophobicity on tensile rheological properties of silica nanoparticle monolayers at the air–water interface. Colloids Surf Physicochem Eng Asp 395:262–266